Figure S1a. Movie of calcium wave propagation

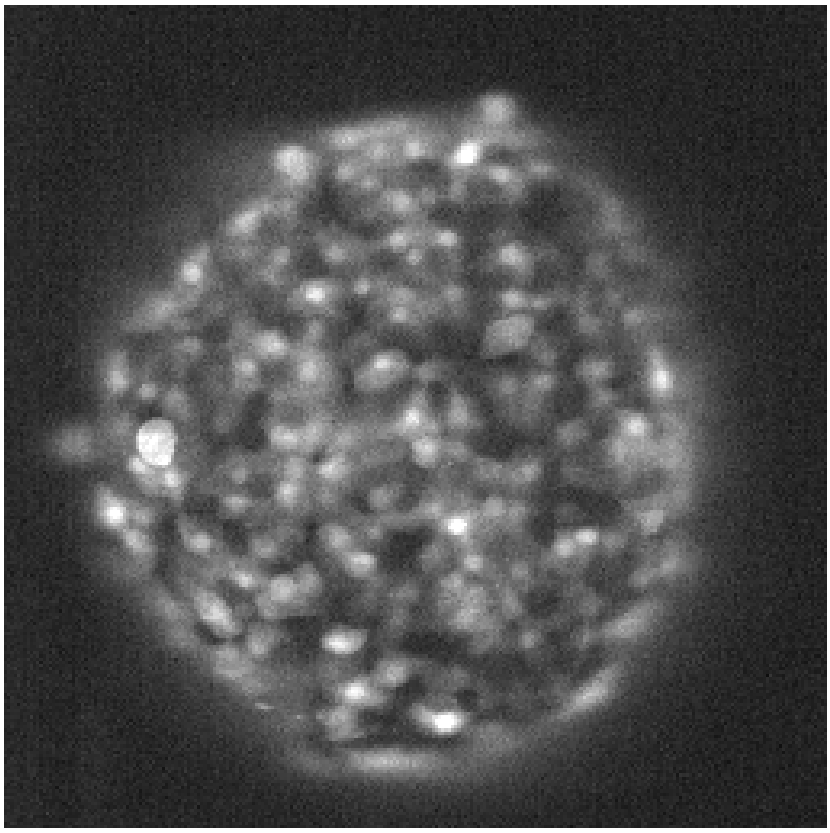

Time lapse movie (see 'supplementary movie 1.avi') of Fluo-4 fluorescence intensity in a WT islet at 11mM glucose stimulation, displayed in figure 1, replayed at ~10 times speed. During oscillations, $[Ca^{2+}]_i$ increases first in cells at the bottom of the islet, then in the middle of the islet and lastly at the top of the islet. These result in a calcium wave that propagates from the bottom to the top of the islet.

Figure S1b. Movie of calcium oscillations in Cx36+/- islet

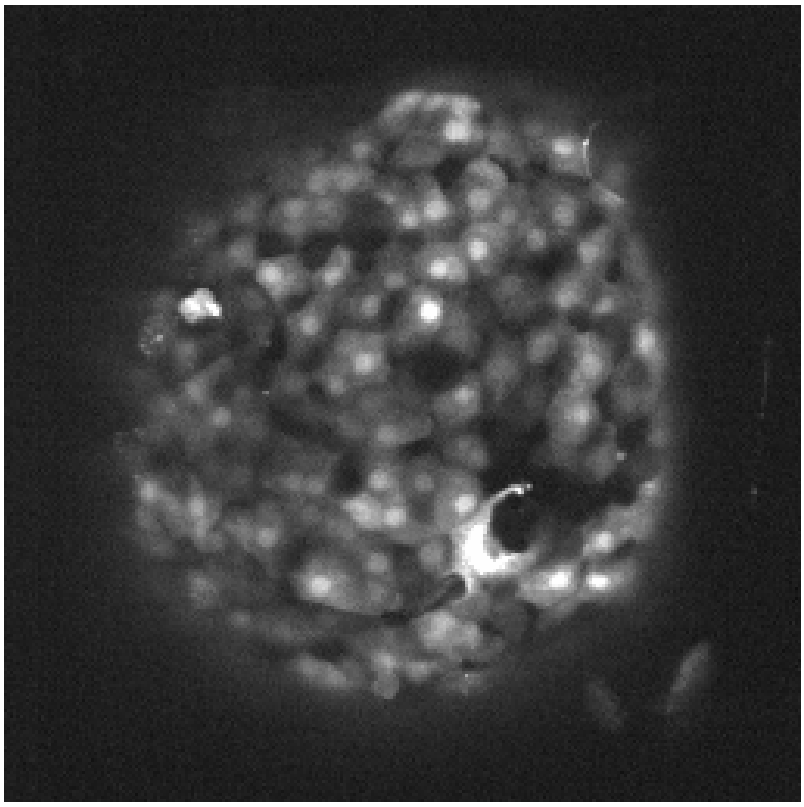

Time lapse movie (see 'supplementary movie 2.avi') of Fluo-4 fluorescence intensity in a Cx36+/- islet at 11mM glucose stimulation, displayed in figure 4a, replayed at ~15 times speed. Only partially synchronized $[Ca^{2+}]_i$ oscillations are visible.

Figure S1c. Movie of calcium oscillations in Cx36-/- islet

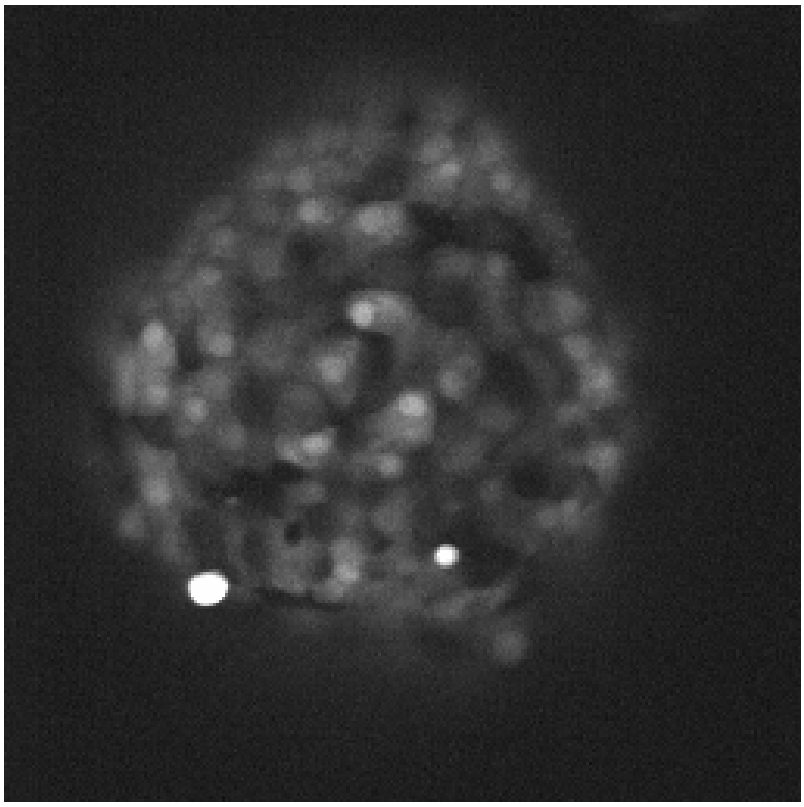

Time lapse movie (see 'supplementary movie 3.avi') of Fluo-4 fluorescence intensity in a Cx36-/- islet at 11mM glucose stimulation, displayed in figure 4c, replayed at ~15 times speed. No synchronized $[Ca^{2+}]_i$ oscillations are visible.

Figure S2. Variation in Cx36+/- behavior between mice

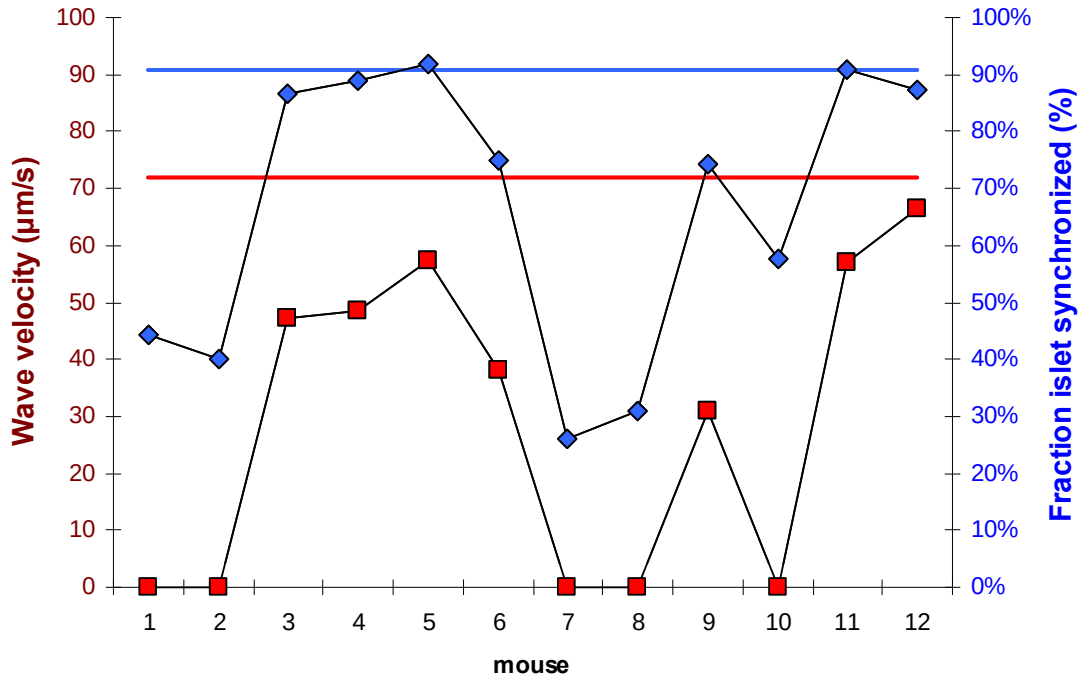

The variation in the measured $[Ca^{2+}]_i$ dynamics at elevated glucose stimulation in islets from Cx36+/- mice. The wave velocity (■) and the fraction of the islet that shows synchronized oscillations (■) show a large variation between different Cx36+/- mice. The wave velocity and synchronization are generally lower than that found for WT control mice (—, — respectively). There is also a strong correlation for a loss in wave propagation (0 wave velocity) coinciding with a low oscillation synchronization.

Figure S3. Origin of waves in regions of higher excitability

Seed 203, g_{KCa} and* r *matrix

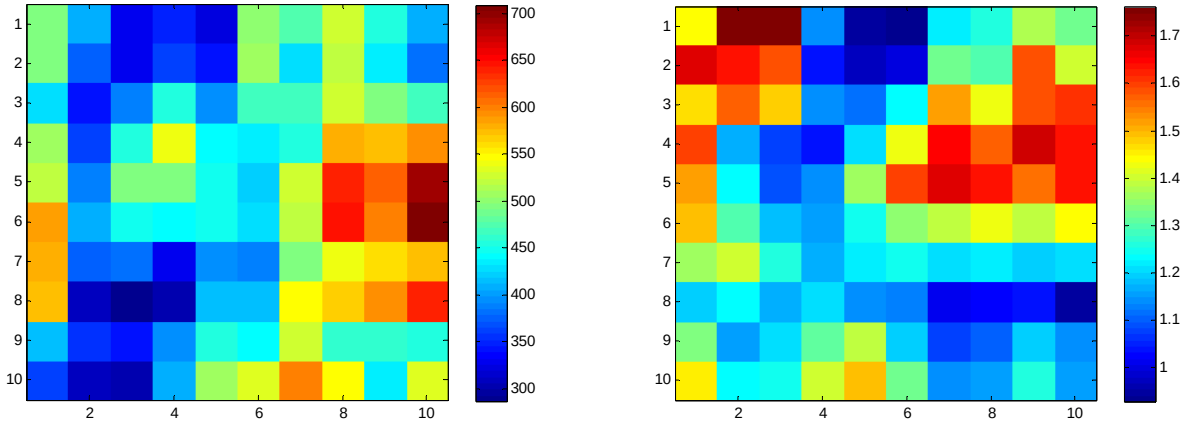

Left: array of g_{KCa} values (with 3x3 smoothing), right: array of **r** values (with 3x3 smoothing). These both correspond to the plane of the islet shown in figure 5b,d,f, representing electrical and metabolic heterogeneity in the islet.

Heterogeneity in g_{KCa} (electrical)

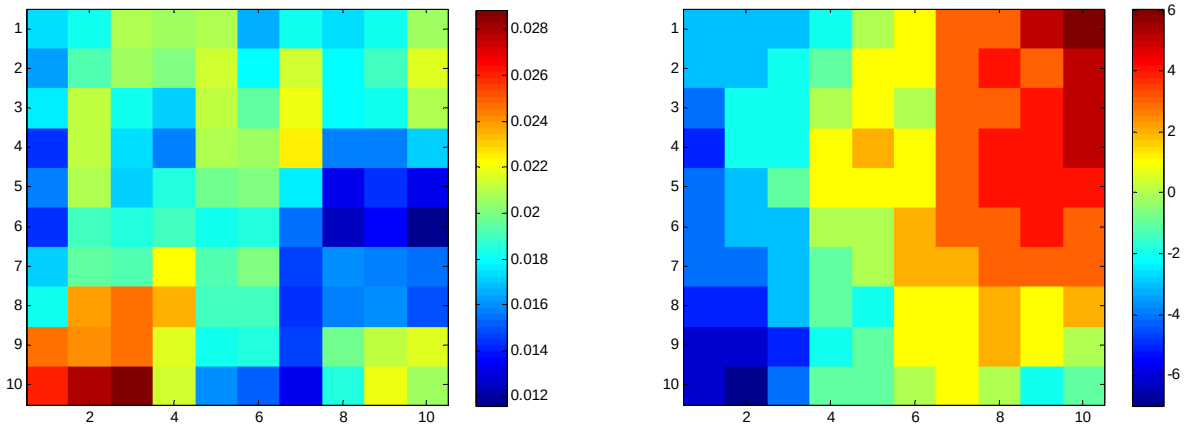

Left: Map of calcium modulation in islet in the absence of gap junction coupling (with 3x3 smoothing). A low modulation indicates that the electrical activity is continually spiking, and corresponds to regions of high g_{KCa}. Upper-right edge of the islet shows the most spiking activity, bottom-left of the islet shows the least. Right: Phase map of Ca wave, where earlier time increases are indicated by a positive time index. The phase map shows that the wave initiates in the red sub-region where there is more spiking activity (increased excitability; high g_{KCa}), and terminates in the blue sub-regions with least spiking activity (lower excitability; low g_{KCa}).

Heterogeneity in* r *and* g_{KCa} *(electrical and metabolic)

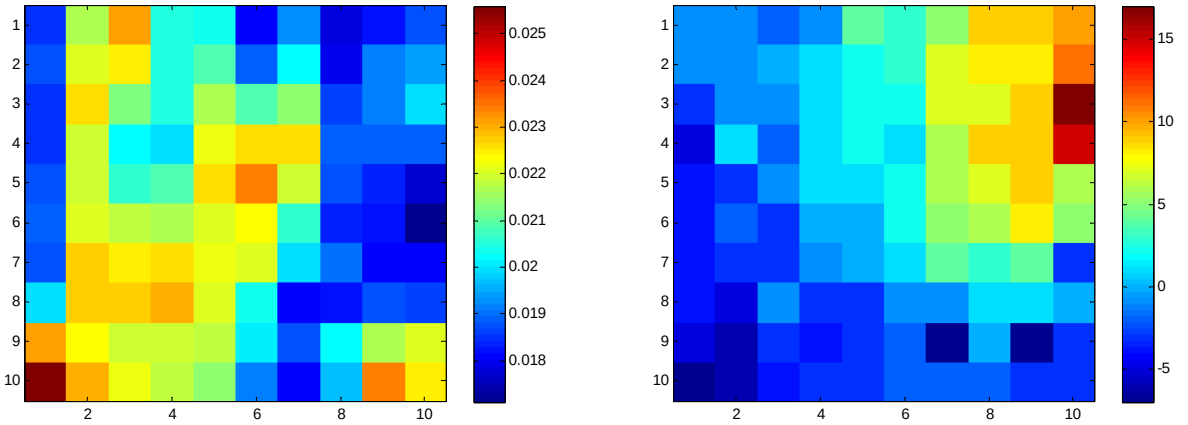

Left: Map of calcium modulation in islet in the absence of gap junction coupling (with 3x3 smoothing). A low modulation indicates that the electrical activity is continually spiking, and corresponds to regions of high g_{KCa} and high **r**. Upper-right edge of islet shows the most spiking activity bottom-left shows the least. Right: Phase map of Ca wave, where earlier increases in $[Ca^{2+}]_i$ are indicated by a positive time index. The phase map shows that the wave initiates in the red sub-region where there is more spiking activity (increased excitability; high **r**, high g_{KCa}), and terminates in the blue sub-regions with least spiking activity (lower excitability; low **r**, low g_{KCa}).

The region at which the wave initiates is slightly towards the edge of the islet from the area of increased excitability. This can be explained by the cubic islet structure used in the phantom-burster model, which leads to edge and corner cells undergoing less electrical clamping from their neighbors, which are therefore more excitable compared to the more coupled cells in the centre of the cubic structure.

This data is representative of 6 modeled islets which show calcium waves that propagate in a consistent direction, each using a g_{KCa}, **r** and g_{coup} parameter distribution generated from different random number generator seeds. The above example show single plane data only where the wave initiates, however this was also consistent throughout the z direction of the modeled islet.

Figure S4. Oscillation synchronization with gap junction coupling in computational model.

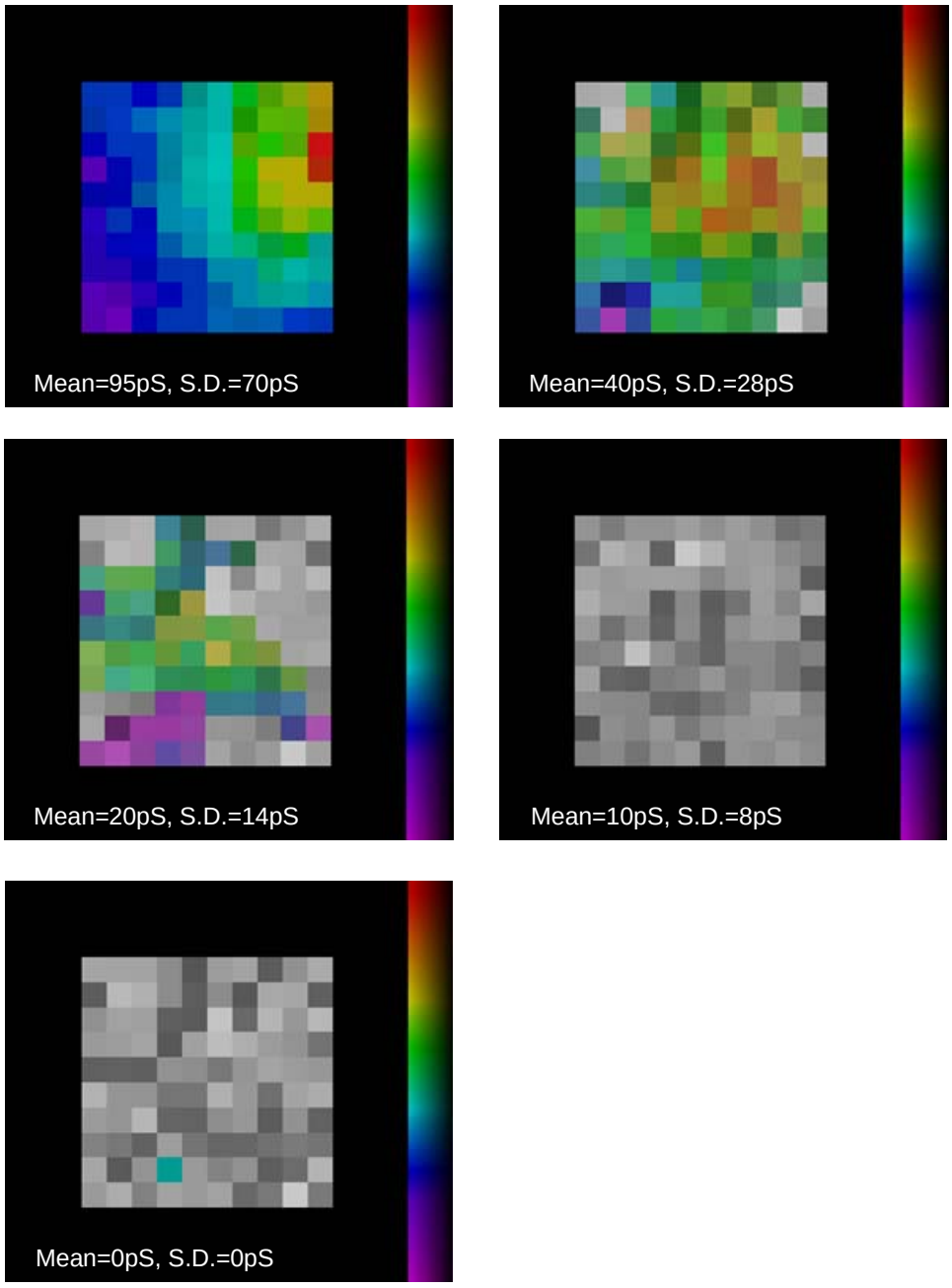

Representative false color scale phase maps of the calcium oscillation phase and synchronization for various distributions of the gap junction coupling conductance. The random number seed is 203, corresponding to that used in figure 5 of the main text, as well as in the data above in section S3. The colorbar represents ±0.5s.

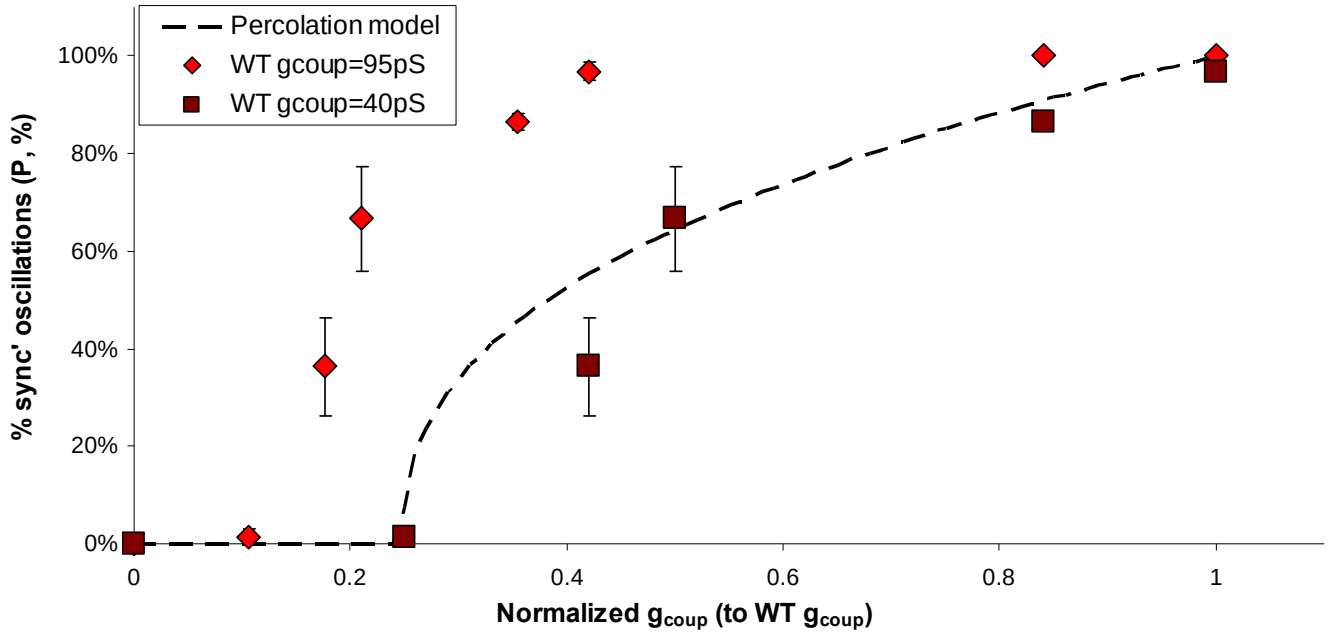

Summary of the results from the computational modeling of the islet under varying gap junction coupling, with a comparison to results predicted by the percolation model of islet connectivity. The mean oscillation synchronization (averaged over 5 random number seeds) is plotted as a function of the mean coupling conductance, normalized to the wild-type mean coupling conductance. If the wild-type coupling conductance is assumed to have a distribution with Mean=95pS, S.D.=70pS, then the oscillation synchronization (red diamonds, ♦) reduces with reduced gap junction coupling until it reaches ~0% at ~10% of the wild-type coupling conductance. This relationship has poor agreement with the percolation model (black dashed line, ---). If however, the wild-type coupling conductance is assumed to have a distribution with Mean=40pS, S.D.=28pS the oscillation synchronization (brown squares, ■) shows a reduction with reduced gap junction coupling in much better agreement with the percolation model. Furthermore, at ~25% of the mean WT gap junction coupling conductance, the oscillation synchronization is almost 0%, with no coordinated oscillations throughout the islet.